


# A novel natural surface-enhanced fluorescence system based on reed leaf as substrate for crystal violet trace detection

Hui-Ju Cao(曹会菊), Hong-Wen Cao(曹红文), Yue Li(李月), Zhen Sun(孙祯), Yun-Fan Yang(杨云帆), Ti-Feng Jiao(焦体峰), and Ming-Li Wang(王明利)

**Citation:**Chin. Phys. B, 2022, 31 (**10**): 107801. DOI: 10.1088/1674-1056/ac7215
Journal homepage: http://cpb.iphy.ac.cn; http://iopscience.iop.org/cpb

**What follows is a list of articles you may be interested in**

---

## Enhanced photoluminescence of monolayer $MoS_2$ on stepped gold structure

Yu-Chun Liu(刘玉春), Xin Tan(谭欣), Tian-Ci Shen(沈天赐), and Fu-Xing Gu(谷付星)
Chin. Phys. B, 2022, 31 (**8**): 087803. DOI: 10.1088/1674-1056/ac657b

## Surface-enhanced fluorescence and application study based on Ag-wheat leaves

Hongwen Cao(曹红文), Liting Guo(郭立婷), Zhen Sun(孙祯), Tifeng Jiao(焦体峰), and Mingli Wang(王明利)
Chin. Phys. B, 2022, 31 (**3**): 037803. DOI: 10.1088/1674-1056/ac1f0d

## Hot spots enriched plasmonic nanostructure-induced random lasing of quantum dots thin film

Feng Shan(单锋), Xiao-Yang Zhang(张晓阳), Jing-Yuan Wu(吴静远), Tong Zhang(张彤)
Chin. Phys. B, 2018, 27 (**4**): 047804. DOI: 10.1088/1674-1056/27/4/047804

## A general method for large-scale fabrication of Cu nanoislands/dragonfly wing SERS flexible substrates

Yuhong Wang(王玉红), Mingli Wang(王明利), Lin Shen(沈琳), Yanying Zhu(朱艳英), Xin Sun(孙鑫), Guochao Shi(史国超), Xiaona Xu(许晓娜), Ruifeng Li(李瑞峰), Wanli Ma(马万里)
Chin. Phys. B, 2018, 27 (**1**): 017801. DOI: 10.1088/1674-1056/27/1/017801

## Interplay between out-of-plane magnetic plasmon and lattice resonance for modified resonance lineshape and near-field enhancement in double nanoparticles array

Ding Pei, Wang Jun-Qiao, He Jin-Na, Fan Chun-Zhen, Cai Gen-Wang, Liang Er-Jun
Chin. Phys. B, 2013, 22 (**12**): 127802. DOI: 10.1088/1674-1056/22/12/127802

---

# A novel natural surface-enhanced fluorescence system based on reed leaf as substrate for crystal violet trace detection

Hui-Ju Cao(曹会菊)[1], Hong-Wen Cao(曹红文)[1], Yue Li(李月)[1], Zhen Sun(孙祯)[1], Yun-Fan Yang(杨云帆)[1], Ti-Feng Jiao(焦体峰)[2,†], and Ming-Li Wang(王明利)[1,‡]

[1] *State Key Laboratory of Materials Science & Technology and Key Laboratory for Microstructural Material Physics of Hebei Province, School of Science, Yanshan University, Qinhuangdao* 066004, *China*

[2] *Hebei Key Laboratory of Applied Chemistry, School of Environmental and Chemical Engineering, Yanshan University, Qinhuangdao* 066004, *China*

(Received 25 April 2022; revised manuscript received 16 May 2022; accepted manuscript online 23 May 2022)

The preparation of surface-enhanced fluorescence (SEF) substrates is often influenced by experimental strategies and factors such as the morphology and size of the nanostructures. In this study, using the natural reed leaves (RLs) without any special pretreatment as the substrate, metal silver is modified by magnetron sputtering technology to prepare a stable and efficient SEF system. The abundant "hedgehog-like" protrusions on the RL substrate surface can generate high-density "hot spots", thus enhancement factor (EF) is enhanced up to 3345 times. The stability and reproducibility are verified in many measurements. The contribution of the intervention of silver nanostructure to the radiation attenuation process of fluorescent molecules is analyzed with the aid of Jablonski diagrams. Three-dimensional (3D) finite difference time domain (FDTD) simulates the spatial electric field and "hot spots" distribution of the substrate. The "hedgehog-like" protrusion structure generates multiple "hot spots", which produce an excellent local surface plasmon resonance (LSPR) effect and provide higher fluorescence signal. Finally, RL/Ag-35 substrate is used to detect crystal violet (CV), and the detection limit is as low as $10^{-13}$ M. This "hedgehog-like" SEF substrate provides a new strategy for the trace detection of CV, which has a good practical application value.

**Keywords:** surface-enhanced fluorescence, biological materials, reed leaf, hot spots

**PACS:** 78.67.–n, 78.55.–m, 73.20.–r **DOI:** 10.1088/1674-1056/ac7215

## 1. Introduction

With the development of technology, fluorescence detection technology has become a widely used convenient detection method.[1] However, owing to the limited luminous intensity of fluorescent molecules, finding a more efficient and sensitive fluorescence detection method has been research hotspots.[2] Surface-enhanced fluorescence (SEF) technology is an effective enhancement strategy that has been rapidly developed in materials science,[3–5] food safety,[6–8] and biosensing[9–11] due to its high efficiency and sensitivity. This strategy depends on the local surface plasmon resonance (LSPR) of noble metal nanostructure to generate local electromagnetic field enhancement near the substrate surface, resulting in enhanced fluorescence signals, and has received more attention from researchers.[12] The LSPR of precious metals such as gold (Au), silver (Ag), and copper (Cu) covers most of the visual and near-infrared range and is commonly used in the preparation of SEF substrates to enhance the fluorescence intensity.[13,14] The high-quality factor properties of Ag and its strong resonance adsorption capability enable Ag to generate good surface plasma excitonic intensity on the surface of material and has been widely used to construct SEF substrates with good fluorescence enhancement.[13,15] For example, Tetyana *et al.*[16] developed a portable fluorescent sensor system based on AgNPs-containing molecularly imprinted polymers (MIP) films, achieving the selective identification of aflatoxin $B_1$ for field applications. Owing to the LSPR phenomenon, comparing with the sensor based on an AgNPs-free MIP sensor chip, the detection limit of this method is reduced by 33 times, and the overall value of sensor response is significantly increased. Sun *et al.*[17] developed a composite fluorescent nanoprobe for the selective and sensitive detection of dopamine based on the metal-enhanced fluorescence effect of gelatin-coated Ag nanoparticles, and a significant fluorescence enhancement effect is achieved.

Because the SEF properties are influenced by the size, morphology, and fluorophore-to-metal distance of nanostructures, various forms of plasma nanostructures (such as nanorods, nanocubes, and core–shell structures[18–20]) are made in an attempt to produce better SEF effects. But usually, these manufacturing processes are time-consuming, low in efficiency, and difficult to control. The hydrophobicity of natural biomaterials comes from their unique micro-nano structures,[21,22] which can provide a suitable environment for the growth of metal nanostructures without any spectral interference. However, there are currently few re-

†Corresponding author. E-mail: tfjiao@ysu.edu.cn
‡Corresponding author. E-mail: wml@ysu.edu.cn

© 2022 Chinese Physical Society and IOP Publishing Ltd 

searches of the direct application of the micro-nano structures of natural biomaterials to SEF. Fortunately, well-defined micro-nano materials in nature have received extensive attention in recent years. Some scientific studies have shown that biological materials such as insect wings, shells, and plant petals/leaves have excellent SEF or SERS (here, SERS stands for surface enhanced Raman scattering) properties and can be used for efficient, multi-component determination of probe molecules.[23–25] The unique "hedgehog-like" protrusions on the surface of RLs provide multiple locations for "hot spots" generation and effectively enhance the fluorescence signal. In addition, in the preparation of SEF substrates, magnetron sputtering technology is a promising nanomaterial growth candidate, and it is easier to manipulate, less damaged, and supports large-scale production than the complex techniques such as electron beam lithography, chemical etching, and impregnation.[26–28]

In summary, the natural biological SEF substrate was successfully used to detect crystal violet (CV). Ag was modified on natural RL surface without special pre-treatment by using the magnetron sputtering technology. By adjusting the sputtering time, a series of substrates with different microscopic morphologies was obtained, which were screened for the best SEF substrate using rhodamine 6G (R6G) solution with a concentration of $10^{-5}$ M. The RL/Ag-35 substrate has an enhancement factor (EF) as large as 3345 times, and many experiments have repeatedly verified that the substrate has good stability and reproducibility. The SEF phenomenon of the substrate is confirmed by theoretical analysis, the "hedgehog-like" protrusions structure distributed on RL substrate surface can generate multiple "hot spots" under Ag modification, which effectively enhances the intensity of the local electric field and produces good LSPR effect, providing higher fluorescence signal. The RL/Ag-35 substrate is used to detect CV with detection limit as low as $10^{-13}$ M. The "hedgehog-like" substrate provides a new strategy for the trace detection of CV and has good practical application value.

## 2. Experiment

### 2.1. Chemicals and materials

The RLs were bought from Teng Guojia yu Trading (Taobao, China). The probe molecule of rhodamine 6G (R6G, $C_{28}H_{31}N_2O_3Cl$) was purchased from J & K Science Co. The crystal violet (CV, $C_{25}H_{30}ClN_3$) was purchased from Tianjin Kemiou Chemical Reagent Co., Ltd. The Ag target (purity 99.99%) used for magnetron sputtering was obtained from China Material Technology Co., Ltd. A custom-made 99.99% pure silica glass bath (400-μm deep) was used for fluorescence intensity measurements by Lianyungang Yuelin Technology Co. The deionized water used to prepare the solution was sourced from the Key Laboratory of Physics of Microstructured Materials in Hebei Province, China.

### 2.2. Instruments

The RL was modified by Ag nanomaterial with a direct-current (DC) magnetron sputtering apparatus (JGP450). The information about morphology of the substrate was characterized by scanning electron microscopy (SEM, Hitachi S4800 II) and x-ray diffraction (XRD, D/Max-2500/PC). The fluorescence spectra of the SEF substrate were recorded by a fluorescence spectrometer (F-7000). The ultraviolet-visible (UV-Vis) absorption spectra of the solution and the substrate were obtained by the ultraviolet spectrophotometer (UV-2550).

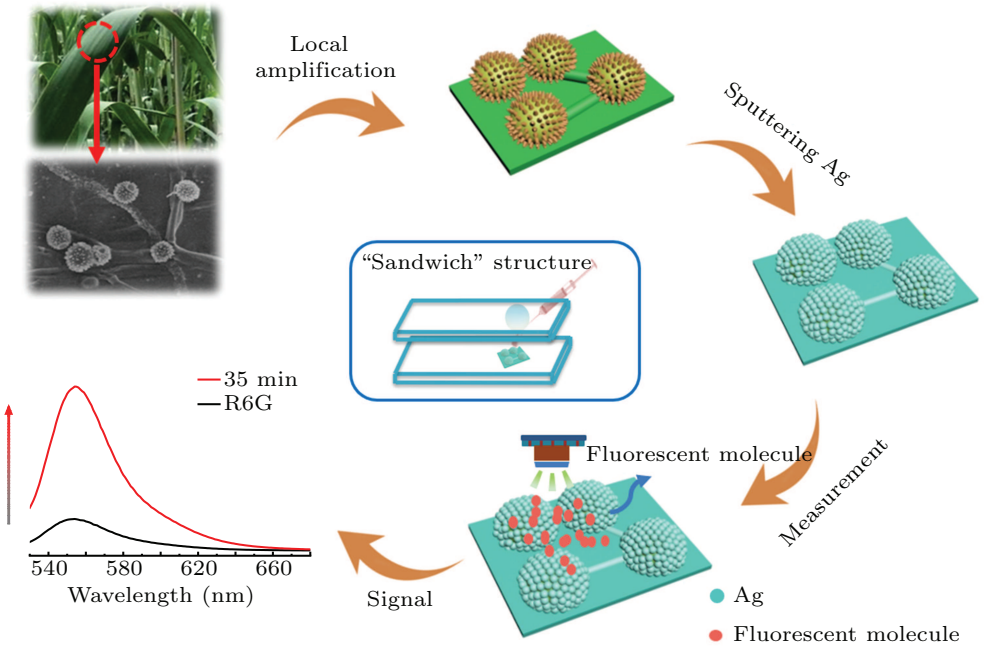



**Fig. 1.** Schematic diagram of preparation and spectra measurement process of RL/Ag substrates.

### 2.3. Sample preparation

The preparation process of the SEF substrate is shown in Fig. 1 in the following sequences: Prepare 1 cm×1 cm-size pieces of RL and rinse them with anhydrous ethanol to remove the impurities from their leaves. After their naturally drying at room temperature, the aluminum sheet was pasted on the processed RL with double-sided tape and the RL was fixed to the glass, then it was processed by the magnetron sputtering of the metallic Ag. The Ag was deposited on the surface of RL by the DC magnetron sputtering instrument with operating parameters of 480 V, 400 mA, and $1.0\times10^{-3}$-Pa argon gas flow. The sputtering times of Ag as 5, 10, 15, 20, 25, 30, 35, and 40 min respectively. The prepared samples were denoted as RL/Ag-X.

## 3. Result and discussion

### 3.1. Characteristics of substrate

The RL is a kind of hydrophobic surface with a hundred-micron period striped grating.[29] Figure 2 shows SEM images of Ag sputtering on the substrate at different times. Figure 2(a) shows the SEM image of unmodified RL. Periodic fringe protrusion structure with micron size can be seen on the surface. As shown in Figs. 2(b)–2(d), the insets display the corresponding diameter distribution histogram of 300 random target measurements on substrates. Figures 2(b) and 2(b1) show the locally magnified SEM images of RL. The microcosmic surface has many protrusions with an average diameter of $2.99\pm0.2$ μm and an average "hedgehog-like" protrusion of $250\pm0.2$ nm in height. Figure 2(c) shows the SEM of the RL/Ag-35 substrate and the successfully modified Ag on substrate surface. The local microscopic magnification of RL/Ag-35 substrate is shown in Fig. 2(c1). After Ag modification, the average diameter of the protrusions is $4.12\pm0.2$ μm, and the average diameter of "hedgehog-like" protrusions is $330\pm0.2$ nm. Figure 2(d) shows the SEM of the RL/Ag-40 substrate. The local microscopic magnification of RL/Ag-40 substrate is shown in Fig. 2(d1). And, the average diameter of the protrusions is $4.33\pm0.2$ μm, and the average diameter of the "hedgehog-like" protrusions is $480\pm0.2$ nm.

Figure 3(a) shows the molecular structure and 3D model of R6G. The aqueous solution of R6G ($10^{-5}$ M) is prepared to screen the best substrate. The UV-Vis absorption spectrum of substrate and fluorescent reagent are measured to select the appropriate excitation light. Figure 3(b) shows the UV-Vis absorption spectrum of R6G, RL/Ag-25, and RL/Ag-35 substrates. The absorption peak of the R6G solution (black line) is at 526 nm. The absorption peak is at 319 nm for the RL/Ag-25 substrate (blue line) and at 321 nm for RL/Ag-35 substrate (red line). The absorption peak of RL/Ag-35 substrate is slightly stronger than that of RL/Ag-25 substrate. And in a range of 470 nm–700 nm, there appears a peak. As shown in Fig. 3(c), The analysis of EDS can reveal the element composition, weight, and atomic percentage of the substrate. There are mainly C and Ag elements in the substrate, specifically, 18.63-at.% C and 81.37-at.% Ag. The XRD pattern of RL/Ag-35 substrate is shown in Fig. 3(d), indicating the values of $2\theta = 38.11°$, 44.33°, 64.38°, and 77.48° are just corresponding to crystallographic planes (111), (200), (220), and (311) of the face-centered cubic Ag phase (JCPDS 04-0783), respectively. All these results indicate that Ag is successfully modified on the RL surface during substrate preparation with introducing no other impurities.

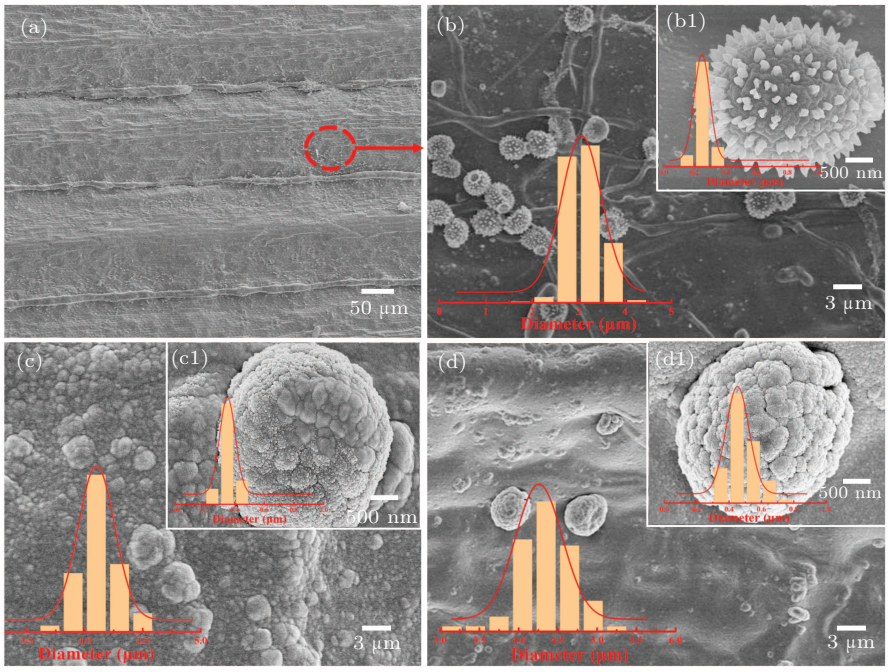



**Fig. 2.** Top-view SEM images of the substrate for [(a) and (b)] unmodified RL, (c) RL/Ag-35, (d) RL/Ag-40. [(b1)–(d1)] Locally enlarged SEM images of RL, RL/Ag-35, and RL/Ag-40. The insets show corresponding diameter distribution histogram of 300 random target measurements on substrates.

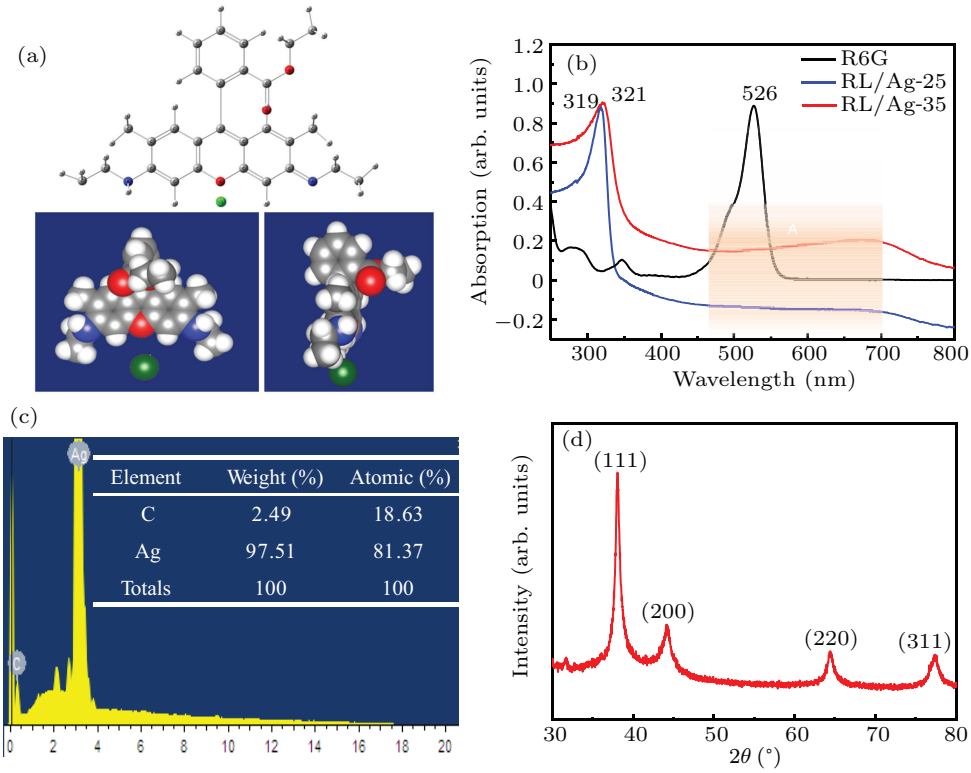



**Fig. 3.** (a) Molecular structure and 3D model of R6G, (b) UV–Vis absorption spectrum of R6G ($10^{-5}$ M), RL/Ag-25, and RL/Ag-35 substrates, (c) EDS image of RL/Ag-35 substrate, and (d) XRD pattern of RL/Ag-35 substrate.

### 3.2. SEF phenomenon and EF calculation

It is generally necessary to detect and analyze the substrate and probe molecules by UV-Vis absorption spectrum before fluorescence detection. The intensity and shape of the fluorescence spectrum are closely related to the incident waveband.[30,31] Absorption spectrum reflects the dependence of molecular absorption intensity on wavelength, which can be used as the basis for selecting excitation wavelength in fluorescence measurement experiments. The excitation light at 500 nm is in the response band of fluorescent molecule and is capable of inducing the SPR effect. Figure 4(a) shows the contact angle formed by dropping R6G solution on reed leave, which is simply photographed and recorded, and the contact angle is about $126° \pm 2°$. The RL is a hydrophobic surface structure. The contact angle of RL/Ag-35 substrate is about $130° \pm 2°$. The RL surface modified by Ag nanomaterials is still hydrophobic. Figure 4(b) shows the actual picture and schematic diagram of "sandwich" structure in the measurement process. During the measurement operation, the "sandwich" structure is placed into the fluorescence spectrometer to detect the fluorescence. To ensure the effectiveness of the results, the fluorescence signal acquisition parameters are the same for each solution and obtained at room temperature. Through measuring, the fluorescence spectra of the substrates are obtained as shown in Fig. 4(c). This figure shows the fluorescence intensity of the R6G at $10^{-5}$ M (black line) and fluorescence intensities of the R6G on different substrates (other colored lines). Without the substrate, the peak of R6G is at 555 nm and the peak of fluorescence intensity is at 623 a.u. When Ag is modified on RL, the fluorescence intensity of R6G solution increases significantly. As the deposition time is less than 35 min, the fluorescence intensity increases with deposition time increasing. At 35 min, the fluorescence intensity of the R6G is the highest. When the Ag deposition time exceeds 35 min, the fluorescence intensity begins to decrease. The peak position of R6G does not change just because of using different substrates in the measurement process. The measurement error bar shows the accuracy of each test. Under multiple measurements, the fluorescence intensity of the substrate has no significant change for the same sputtering time. The EF is an important way of measuring the enhancement properties of a substrate. The EF is investigated for substrates with metals deposited for different times and it is expressed as the general formula below:[32]

$$\mathrm{EF} = \frac{I_{\mathrm{Ag-substrate}}}{I_{\mathrm{R6G}}}, \tag{1}$$

where $I_{\mathrm{Ag-substrate}}$ is the fluorescence intensity of RL/Ag-35 substrate, and $I_{\mathrm{R6G}}$ represents the fluorescence intensity of R6G on a pure glass substrate. Figure 4(d) shows the calculated relationship between EF and magnetron sputtering time. The substrate EFs at the sputtering time of 5 min–45 min are 2.81, 3.28, 3.87, 4.08, 4,43, 4.82, 5.18, 3.63, and 2.57, respectively.

However, the distance between fluorescent molecule and metal nanoparticle is a key factor in the enhancement of SEF

detection.[33,34] When molecules are too close to or direct contact with metal nanoparticles, fluorescence will quench. On the contrary, when the molecules are too far from the metal, the local electromagnetic field created by the LSPR will be unable to act on the fluorescent molecules and the substrate enhancement effect will not be obvious.[35,36] In our experiments, the groove of custom silicon glass is 400-μm deep. However, fluorescent molecules can be enhanced only in 20-nm-deep metal. Most of fluorescent molecules cannot produce the SEF effect, so it is necessary to correct the EF. According to Zhang *et al.*'s work,[34] EF correction can be calculated from the following formula:

$$0.5X + 399.5Y = 400 \cdot \mathrm{EF} \cdot Y, \tag{2}$$

$$\mathrm{EF_{cor}} = \frac{X}{Y}, \tag{3}$$

where $X$ is the fluorescence enhancement intensity per micron in the matrix, $Y$ is the fluorescence enhancement intensity per micron of the unenhanced R6G aqueous solution in the intercalated structure, and $\mathrm{EF_{cor}}$ denotes the correct enhancement factor. The calculated values of $\mathrm{EF_{cor}}$ of RL/Ag-X substrate are shown in Table 1. The fluorescence intensity of RL/Ag-35 substrate can be enhanced up to 3345 times, and the substrate has an excellent SEF effect.

**Table 1.** Calculated values of EF and $\mathrm{EF_{cor}}$ of different RL/Ag-X substrates.

| Substrate | EF | $\mathrm{EF_{cor}}$ |
|---|---|---|
| RL/Ag-5 | 2.81 | 1449 |
| RL/Ag-10 | 3.28 | 1825 |
| RL/Ag-15 | 3.87 | 2297 |
| RL/Ag -20 | 4.08 | 2465 |
| RL/Ag-25 | 4.43 | 2745 |
| RL/Ag-30 | 4.82 | 3057 |
| RL/Ag-35 | 5.18 | 3345 |
| RL/Ag-40 | 3.63 | 2105 |
| RL/Ag-45 | 2.57 | 1257 |

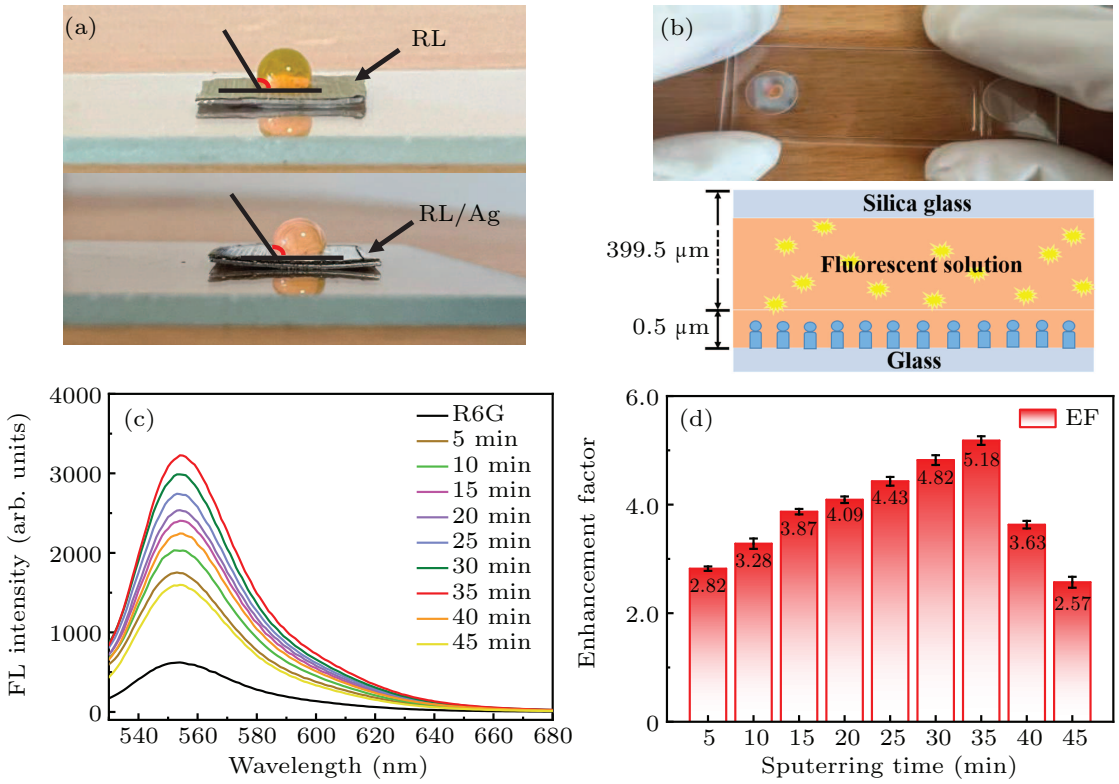



**Fig. 4.** (a) Photo of R6G ($10^{-5}$ M) solution dripping on RL surface and RL/Ag-35 substrate, (b) operating device and schematic diagram of the "sandwich" structure for fluorescence measurement, (c) fluorescence spectra of R6G ($10^{-5}$ M) solution on RL/Ag-X substrates, and (d) EF of R6G ($10^{-5}$ M) solution on RL/Ag-X substrate.

### 3.3. SEF analysis of RL/Ag substrate

As is well known, fluorescence is produced when fluorescent molecule is stimulated by external light and jumps from the ground state to the excited state and then from the excited state $S_1$ back to the ground state $S_0$. Figure 5 shows the schematic and Jablonski energy level transition diagram in the cases without metal (Fig. 5(a) and with metal (Fig. 5(b)). When the LSPR resonance peak frequency of the metal nanoparticles coincides with that corresponding to the emission wavelength of the fluorescent material, they are coupled with each other and improve the radiation emissivity of fluorescent molecules.[37] When the fluorescent molecule and metal mutually interact, the intrinsic radiation decay rate of the fluorescent molecule increases by the influence of the metal. In the state without metal surface storage, the radiation decay rate and radiation-free decay rate are denoted by $\Gamma$ and $k_{\mathrm{nr}}$, re-

spectively, and related to quantum yields $Q_0$ and lifetimes $\Gamma_0$ by[38]

$$Q_0 = \frac{\Gamma}{\Gamma + k_{\rm nr}}, \tag{4}$$

$$\Gamma_0 = \frac{1}{\Gamma + k_{\rm nr}}. \tag{5}$$

In the presence of metal, the radiation-free decay rates of fluorescent molecules are denoted by $\Gamma_{\rm m}$ and $k_{\rm nr}$, respectively, and their quantum yield $Q_{\rm m}$ and lifetime $\Gamma_{\rm m}$ can be expressed as

$$Q_{\rm m} = \frac{\Gamma + \Gamma_{\rm m}}{\Gamma + \Gamma_{\rm m} + k_{\rm nr}}, \tag{6}$$

$$\Gamma_{\rm m} = \frac{1}{\Gamma + \Gamma_{\rm m} + \Gamma_{\rm nr}}. \tag{7}$$

From the above formulas, it can be seen that the radiation decay rate increases as $\Gamma + \Gamma_{\rm m}$ increases after the introduction of the metal surface, and as $\Gamma_{\rm m}$ becomes larger, the quantum yield becomes larger and the fluorescence intensity increases.

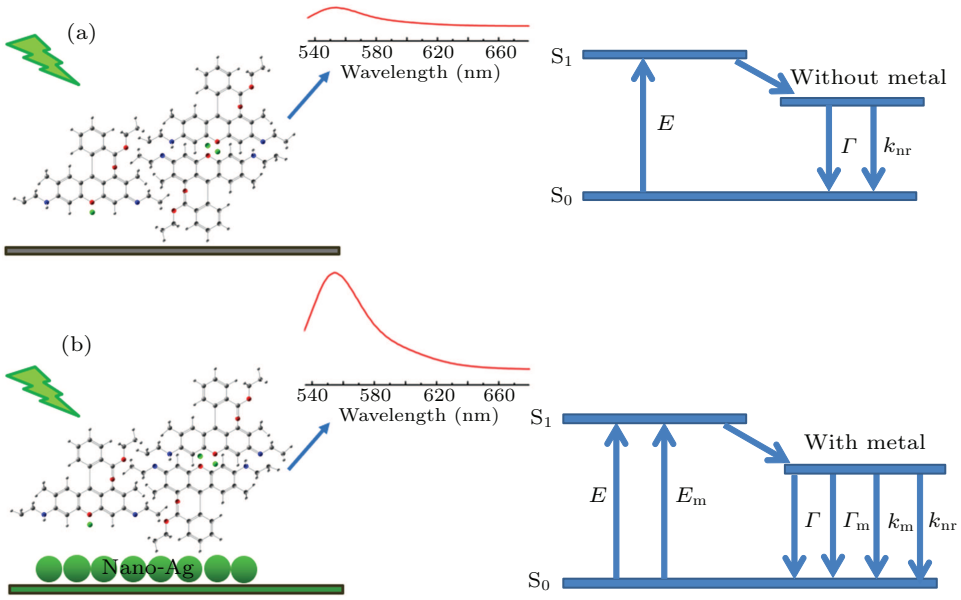



**Fig. 5.** Schematic and Jablonski diagram without (a) and with (b) effects near metal surface.

In addition, when fluorescent molecules are in the neighbourhood of metal nanoparticles, the enhanced electromagnetic field can considerably change the excitation and emission processes of the fluorophore, resulting in enhanced fluorescence.[39] The LSPR generated by the excitation light interacting with Ag nanoparticles on the substrate can promote the absorption of excitation light and increase the absorption efficiency of fluorescent molecules.[35] Furthermore, Mie scattering theory states that when the incident wavelength is fixed and the laser is incident on a homogeneous medium, the fluorescence enhancement is dominated by the scattering cross-section and the fluorescence quenching is determined by the absorption cross-section.[40] In experiment, the increase in size of the Ag nano-islands with increasing metal deposition time leads to the increase in the scattering cross-section and thus in the fluorescence intensity. Nevertheless, as the sputtering time increases, fewer fluorescent molecules enter into the interstices of the Ag nanostructures and the total number of fluorescent molecules excited decreases, the electromagnetic field is enhanced. The luminescence intensity of the fluorescent molecules is not further enhanced. Many "hedgehog-like" structures on the RL surface provide a multi-area environment for growing the Ag nanoparticles. The existence of Ag nanomaterials can effectively enhance the radiation attenuation process of fluorescent molecules and enhance the fluorescence signal.

When light illuminates a rough metallic surface, "hot spots" can appear, where the light is concentrated on a nanometre scale, producing an intense electromagnetic field.[41] "Hot spots" preferentially appear in gaps, cracks or sharp features of plasma materials, generating strong electromagnetic fields and enhancing the luminescence of nearby fluorophores.[8,41] Because "hot spots" are associated with local electromagnetic modes, it is necessary to analyze the electric field distribution on the substrate surface. The 3D-FDTD is commonly used to simulate the spatial field distribution of the local electric field on rough surface of precious metal.[12,30,42] Simulation of the SEF substrate is carried out in conjunction with SEM to analyze the details of "hot spots" distribution and electromagnetic enhancement on the nanostructure of the RL/Ag-35 substrate. The model for the simulation analysis is constructed according to the SEM of the RL and RL/Ag-35 substrates as shown in Fig. 6(a). The wavelength of the incident laser is 500 nm, the ***K*** direction is per-

pendicular to the surface, and the polarization direction of the laser is ***E*** direction. The color near the "hot spots" represents the strength of the electromagnetic field, where the red-like color represents a strong electromagnetic field and the blue-like color refers to a weak electromagnetic field. The simulation is carried out from three planes $P_1$, $P_2$, $P_3$ ($P_1$ corresponds to $X$–$Z$ plane, $P_2$ corresponds to $X$–$Y$ plane, $P_3$ corresponds to $Y$–$Z$ plane) as indicated in Fig. 6(b). As shown in Fig. 6(c), after Ag modification, the "hedgehog-like" protrusions on the RL surface produces high-density "hot spots", and the local field at the "hot spots" is significantly enhanced. In Fig. 6(d), the "hot spots" in regions I and II mainly come from the adjacent "hedgehog-like" protrusions after Ag modification. "Hot spots" in region III are between adjacent spherical structures on the substrate. "Hot spots" in region IV are observed in the $P_2$ plane as shown in Fig. 6(e). The "hot spots" on the RL/Ag-35 substrate surface are distributed not only on the top, side and bottom, but also between adjacent spherical structures. The large number of "hot spots" on the substrate plays an important role in the electromagnetic effect and enhancement of fluorescence signal. The calculations show that the "hedgehog-like" structure of RL is very meaningful. The "hedgehog-like" structure is modified with Ag bring high-density "hot spots" and effectively enhance the electric field. Compared with other structure of biomaterials, such as flower-like nanostructures,[24] sheet-like protrusions,[8] and grating structures,[30] the "hedgehog-like" structure of RL surface results in a stronger local field, a greater density of "hot spots" and a higher fluorescence EF. The unique natural nanostructure of RL provides a prerequisite for producing SEF, which is different from flower-like and other structures.

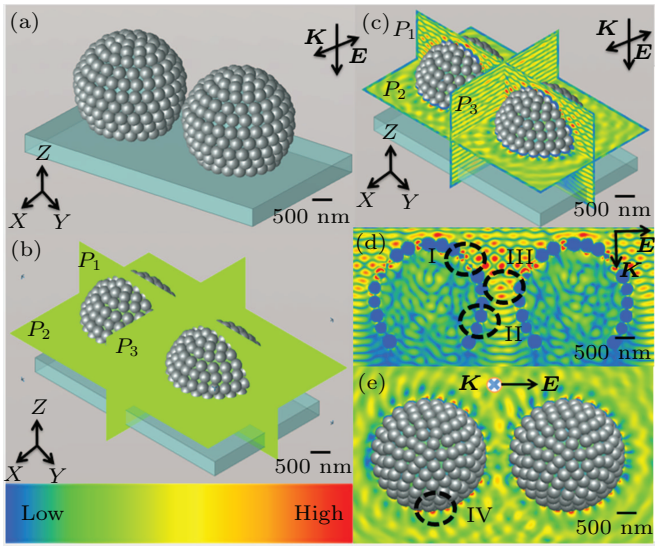



**Fig. 6.** (a) The 3D-FDTD model of RL/Ag-35 substrate, (b) calculated planes of substrate, (c)–(e) spatial distribution of electric field strength for planes $P_1$, $P_2$, and $P_3$.

### 3.4. Reproducibility and stability of RL/Ag-35 substrate

Reproducibility and stability can reflect the practical applications and commercial values of the substrate.[25,30] Excellent reproducibility and stability can reduce experimental cost and error. Experimentally, we measure the reproducibility and stability of the substrate, and the results are shown in Fig. 7. Ten points are randomly selected on the substrate for measuring the fluorescence spectra, and the results are shown in Fig. 7(a). The peak positions of the R6G remain unchanged, and the peak strengths do not change significantly. A relative standard deviation (RSD) formula is given to evaluate the reproducibility of the substrate:[43]

$$\mathrm{RSD} = \frac{\sqrt{\frac{\sum_{i=1}^{n}(I_I - \bar{I})^2}{n-1}}}{\bar{I}}, \tag{8}$$

where $I$ is the measured fluorescence intensity, and $n$ represents the number of measurements. The calculations indicate that the average fluorescence intensity of 10 measurements is 3281 (a.u.) and the RSD value is 4.12% as shown in Fig. 7(b). Thus, as shown in SEM, the large number of dense "hedgehog-like" protrusions on the substrate surface provides the prerequisite for the growth of Ag nanoparticles, resulting in the high-density "hot spots" and showing the good reproducibility. The low RSD values indicate that the "hedgehog-like" structures are uniformly distributed on the substrate surface. The RL/Ag-35 substrate has good reproducibility. As shown in Fig. 7(c), we measure the temporal stabilities of the substrates that have been exposed to air for 0–4 weeks, and record the results, respectively. Figure 7(d) shows that the fluorescence intensity of R6G on the substrate decreases by 4.14% for the substrate that has been exposed to air for one week. After the second week of placement, the fluorescence intensity decreases by 7.43%. When the substrate is exposed to air for 3 and 4 weeks, the fluorescence intensities of the R6G drop by 14.43% and 20.26%, respectively. The fluorescence intensity decreases as the sample is slightly oxidized on the substrate surface with the exposure time to air increasing to 4 weeks and more, but the SEF effect is still present. The RL/Ag-35 substrate has good temporal stability. Owing to the rapid drop in fluorescence intensity after 2 weeks of exposure to air, storage of the substrate in a vacuum bag may be considered to slow down the oxidation process after sample measurement.

### 3.5. Application of the RL/Ag-35 substrate

Crystal violet (CV) is a triphenylmethane fluorescent dye. Its molecular structure and 3D model are shown in Fig. 8(a). It is toxic and labelled as a stubborn toxic carcinogen due to its non-biodegradability, persistence in various environments, and poor microbial metabolism. The Ministry of Agriculture lists it as a prohibited drug in aquatic products.[44,45]

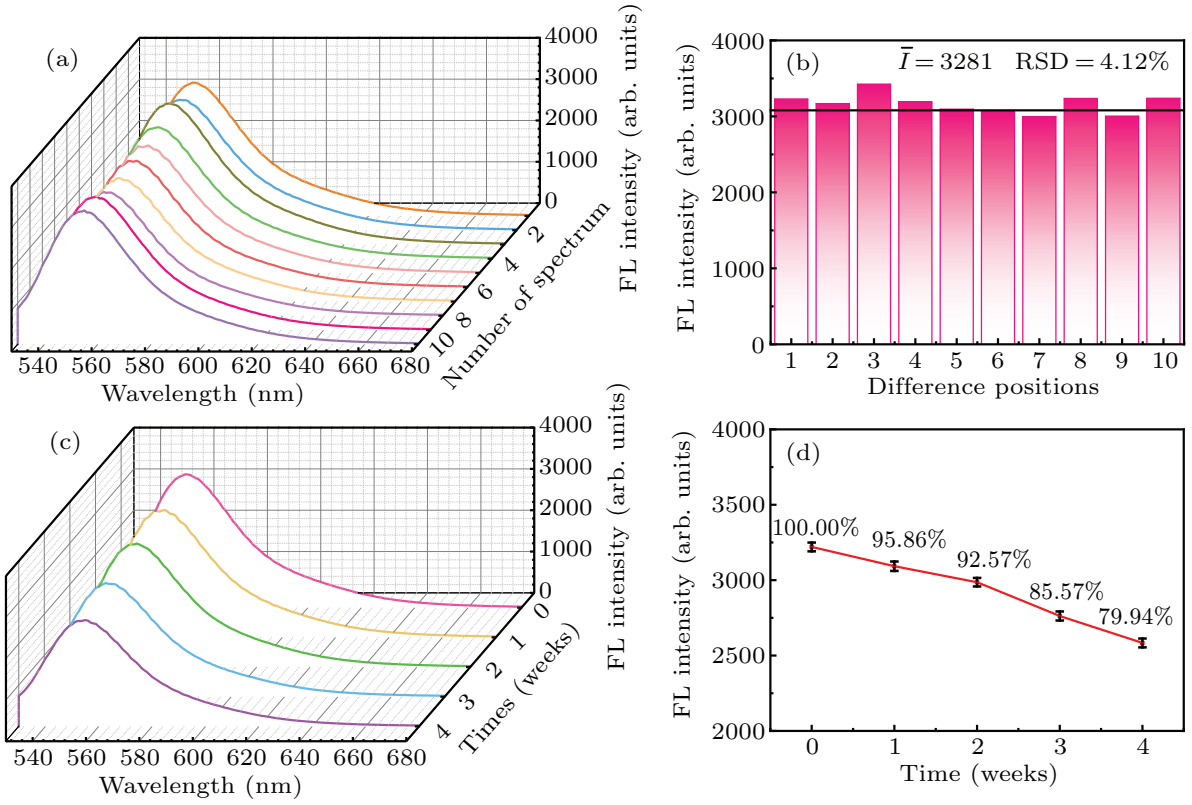



**Fig. 7.** (a) Fluorescence spectra at different positions of R.L./Ag-35 substrate, (b) fluorescence intensities at different measuring positions at 555 nm, (c) fluorescence spectra at different times of RL/Ag-35 substrate, and (d) fluorescence intensities measured at different times at 555 nm.

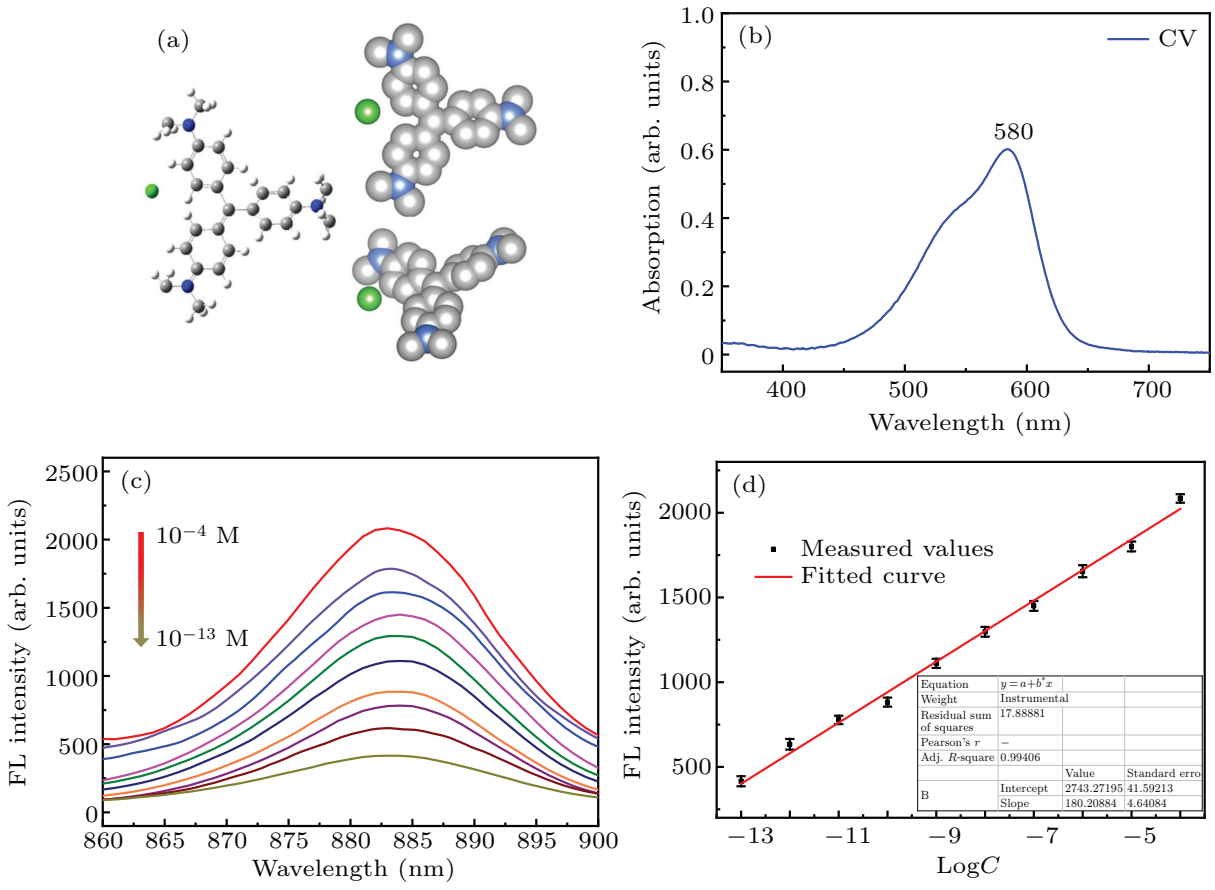



**Fig. 8.** (a) Molecular structure of CV and 3D model of R6G, (b) UV–Vis absorption spectrum of CV, (c) fluorescence spectra of CV ($10^{-13}$ M–$10^{-4}$ M) at different concentrations on the RL/Ag-35 substrate, and (d) linear calibration diagram of fluorescence intensity at different CV concentrations.

**Table 2.** Comparison of different methods of CV detection.

| Technique | Main experimental materials | Material structure | Linear range | Detection limit | References |
|---|---|---|---|---|---|
| SERS | GO/AgNPS/Cu | coated popcorn-like Agnanoparticles | $10^{-3}$ M–$10^{-8}$ M | $10^{-8}$ M | [46] |
| SEF | optical disk, Ag | grating | $10^{-4}$ M–$10^{-10}$ M | $10^{-10}$ M | [30] |
| Fluorescence | $Pb^{2+}$, DNA zyme | dsDNA nanobridge | 10 nM–250 nM | 10 nM ($10^{-5}$ M) | [47] |
| SERS | Au–Ag alloy NPs colloidal suspension | Au–Ag alloy nanochains array | $10^{-7}$ M–$10^{-10}$ M | $10^{-10}$ M | [48] |
| SERS | PVA–AgNP | hydrogel | $10^{-7}$ M–$10^{-13}$ M | $10^{-12}$ M | [49] |
| SEF | reed leaf, Ag | hedgehog-like protrusions | $10^{-4}$ M–$10^{-13}$ M | $10^{-13}$ M | this work |

Therefore, a reasonable, simple, and sensitive CV detection method is crucial. The RL/Ag-35 substrate is used to detect CV. As shown in Fig. 8(b), the absorption peak of CV is first measured before detection, and 580-nm excitation light is selected and serves for the detection light source. Figure 8(c) shows the fluorescence spectra of CV at different concentrations on the substrate, with the detection limits of CV as low as $10^{-13}$ M. Figure 8(d) shows the linear relationship $I = 180.21 \log C + 2743.27$ with the linearity coefficient $R^2 = 0.994$. The assay is linearly correlated in the range of $10^{-13}$ M–$10^{-4}$ M. As shown in Table 2, our experimental strategy provides a wider range of detection of CV and a lower detection line than the methods reported in other researches. More importantly, the method is simple to manipulate and inexpensive as well. Therefore, the RL/Ag-35 substrate can be used to effectively detect CV and has practical application value.

## 4. Conclusions

In summary, a natural biological SEF substrate is successfully used to detect CV. Many "hedgehog-like" protrusions on the RL surface provide the prerequisite for the distribution of Ag nanoparticles on the substrates and bring high-density "hot spots". A series of substrates with different microscopic morphologies is obtained by adjusting sputtering time, and the substrate with the best SEF effect is screened by using R6G solution. The EF of the substrate increases up to 3345 times, and several experimental iterations verify that the substrates have good stabilities and reproducibilities. The combination of the measurements with 3D-FDTD theoretical simulation analysis confirms that the SEF phenomenon of the substrate appears under the modification of Ag, and "hedgehog-like" protrusions distributed on RL surface produces multiple "hot spots", which generate an excellent LSPR effect and provides a higher fluorescence signal. This "hedgehog-like" SEF substrate presents a new strategy to detect CV, with the detection limits as low as $10^{-13}$ M, and has good practical application value.

## Acknowledgements

Project supported by the National Natural Science Foundation of China (Grant Nos. 11674275, 21872119, 22072127, and 12104392) and the Science and Technology Project of Hebei Education Department, China (Grant No. ZD2019069 and QN2021142)).

## References

[1] Zhang Y, Li S, Zhang H and Xu H W 2021 *Bioconjug. Chem.* **32** 4
[2] Cui L, Li R, Mu T, Wang J, Zhang W and Sun M Spectrochim 2022 *Spectrochim. Acta A Mol. Biomol.* **264** 120283
[3] Liu X, Wang R, Ma J, Zhang J, Jiang P, Wang Y and Tu G 2021 *J. Mater. Sci. Technol.* **69** 89
[4] Fereja S, Li P, Guo, Fang Z, Zhang Z, Zhuang Z, Zhang X, Liu K and Chen W 2021 *Talanta* **233** 122469
[5] Omidvar A, RashidianVaziri M R, Jaleh B, Partovi Shabestari N and Noroozi M 2016 *Chin. Phys. B* **25** 118102
[6] Yu L, Chen H, Yue J, Chen X, Sun M, Hou J, Alamry K A, Marwani H M, Wang X and Wang S 2020 *Talanta* **207** 120297
[7] Thao N T, Hoang T X, Phan T B, Kim J Y, Ta H K T, Trinh K T L and Tran N H T 2021 *Dalton Trans.* **50** 6962
[8] Cao H, Guo L, Sun Z, Jiao T and Wang M 2022 *Chin. Phys. B* **31** 037803
[9] Della Ventura B, Gelzo M, Battista E, Alabastri A, Schirato A, Castaldo G, Corso G, Gentile F and Velotta R 2019 *ACS Appl. Mater. Interface* **11** 3753
[10] Kannegulla A, Liu Y, Wu B and Cheng L J 2018 *J. Phys. Chem. C* **122** 770
[11] Choi J H, Lim J, Shin M, Paek S H and Choi J W 2021 *Nano Lett.* **21** 693
[12] Yang R, Cheng Y and Sun M 2021 *Opt. Commun.* **498** 127224
[13] Badshah M A, Koh N Y, Zia A W, Abbas N, Zahra Z and Saleem M W 2020 *Nanomaterials* **10** 1749
[14] Wang B 2020 *Chin. Phys. B* **29** 045202
[15] Strobbia P, Languirand E and Cullum B M 2015 *Opt. Eng.* **54** 100902
[16] Sergeyeva T, Yarynka D, Lytvyn V, Demydov P, Lopatynskyi A, Stepanenko Y, Brovko O, Pinchuk A and Chegel V 2022 *Analyst* **147** 1135
[17] Sun J, Feng A, Wu X, Che X and Zhou W 2021 *Talanta* **231** 122334
[18] Lu X, Lee S, Kim J, Abbas N, Badshah M A and Kim S M 2021 *Biosens. Bioelectron.* **175** 112881
[19] Zhang Y, Chen W, Fu T, Sun J, Zhang D, Li Y, Zhang S and Xu H 2019 *Nano Lett.* **19** 6284
[20] Wang S, He D, Wang Y, Hu Y, Duan, Fu M and Wang W 2014 *Chin. Phys. B* **23** 097803
[21] Hao Z, Li N, Cao H, Guo L, Cao H, Li N, Cao L, Liu H, Jiao T and Wang M 2022 *J. Lumin.* **243** 118684
[22] Yao L, Dai P, Ouyang L and Zhu L 2021 *Microchem. J.* **160** 105728
[23] Li N, Hao Z, Cao H, Guo L, Cao H, Li N, Yang Y, Jiao T, Liu H and Wang M 2022 *Opt. Laser. Technol.* **148** 107765
[24] Chou S, Yu C, Yen Y, Lin K, Chen H and Su W 2015 *Anal. Chem.* **87** 6017
[25] Guo L, Cao H, Cao L, Yang Y and Wang M 2022 *Opt. Commun.* **510** 127921
[26] Wang R, Yan X, Ge B, Zhou J, Wang M, Zhang L and Jiao T 2020 *ACS Sustain. Chem. Eng.* **8** 4521
[27] Ma Y, Shao J, Zhang Y, Lu B, Zhang S, Sun Y, Qu X and Chen Y 2015 *Chin. Phys. B* **24** 080702
[28] He Y, Wang R, Jiao T, Yan X, Wang M, Zhang L, Bai Z, Zhang Q and Peng Q 2019 *ACS Sustain. Chem. Eng.* **7** 10888
[29] Jiang H, Liu Y, Zhang Y, Liu Y, Fu X, Han D, Song Y, Ren L and Sun H 2018 *ACS Appl. Mater. Interfaces* **10** 18416

[30] Wang M, Shang Z, Yan X, Shi G, Cao H, Ma W and Jiao T 2021 *Opt. Commun.* **481** 126522
[31] Li M, Cushing S K and Wu N 2015 *Analyst* **140** 386
[32] Dong J, Zheng H, Yan X, Sun Y and Zhang Z 2012 *Appl. Phys. Lett.* **100** 051112
[33] Liaw J, Tsai H and Huang C 2012 *Plasmonics* **7** 543
[34] Zhang Y, Yang C, Zhang G, Peng Z, Yao L, Wang Q, Cao Z, Mu Q and Xuan L 2017 *Opt. Mater.* **72** 289
[35] Li J, Li C and Aroca R 2017 *Chem. Soc. Rev.* **46** 3962
[36] Dragan A I, Bishop E S, Casas-Finet J R, Strouse R J, McGivney J, Schenerman M A and Geddes C D 2012 *Plasmonics* **7** 739
[37] Shan F, Su D, Li W, Hu W and Zhang T 2018 *AIP Adv.* **8** 025219
[38] Lukomska J, Malicka J, Gryczynski I, Leonenko Z and Lakowicz J R 2005 *Biopolymers* **77** 31
[39] Li M, Liu H and Ren X 2017 *Biosens. Bioelectron.* **89** 899
[40] Aslan K, Leonenko Z, Lakowicz J R and Geddes C D 2005 *J. Fluoresc.* **15** 643
[41] Cang H, Labno A, Lu C, Yin X, Liu Mi, Gladden C, Liu Y and Zhang X 2011 *Nature* **469** 385
[42] Yang L, Xiang X, Miao X, Li L, Yuan X, Yan Z, Zhou G, Lv H, Zheng W and Zu X 2016 *Chin. Phys. B* **25** 014210
[43] Zheng H, Xue H, Zhang Y and Shen Z 2001 *Biosens. Bioelectron.* **17** 541
[44] Lin S, Zhang X, Zhao W, Chen Z, Du P, Zhao Y, Wu Z and Xu H 2018 *Chin. Phys. B* **27** 028707
[45] Vithalkar S H and Jugade R M 2020 *Mater. Today* **29** 4
[46] Zhang M, Chen Z, Wang Z, Zheng Z and Wang D P 2019 *J. Mater. Res.* **17** 2935
[47] Zhou J, Qing M, Ling Y, Wang L, Li N and Luo H 2021 *Sens. Actuators B Chem.* **340** 129968
[48] Dong J, Zhao K, Wang Q, Yuan J, Han Q, Gao W, Wang Y, Qi J and Sun M 2021 *Opt. Express* **29** 36857
[49] Wu C, Li F, Lv F, Yao P, Bi M and Xue T 2021 *Mater. Res. Express* **8** 015008